Research Square

Preprints are preliminary reports that have not undergone peer review.
They should not be considered conclusive, used to inform clinical practice,
or referenced by the media as validated information.

Time-dependent spinal cord pathology defines a one-month window for established experimental cervical spondylotic myelopathy models in rats

[redacted]

sunxin20088@126.com

Affiliated Hospital of Guangdong Medical University

[redacted]

Affiliated Hospital of Guangdong Medical University

[redacted]

Affiliated Hospital of Guangdong Medical University

[redacted]

Sun Yat-sen University

[redacted]

Affiliated Hospital of Guangdong Medical University

[redacted]

Affiliated Hospital of Guangdong Medical University

[redacted]

Affiliated Hospital of Guangdong Medical University

Research Article

Keywords: cervical spondylotic myelopathy, chronic compression, temporal progression, critical window, ultrastructural pathology

Posted Date: September 8th, 2026

DOI: https://doi.org/10.21203/rs.3.rs-10655123/v1

License: This work is licensed under a Creative Commons Attribution 4.0 International License.
Read Full License

Additional Declarations: No competing interests reported.

Abstract

Objective:

The temporal pathology of cervical spondylotic myelopathy (CSM) remains insufficiently defined. This study systematically characterized temporal neurological, histological, and ultrastructural changes in a rat model of chronic cervical spinal cord compression to define a potential pathological window of disease progression.

Methods:

Thirty Sprague–Dawley rats were randomly allocated to a sham-operated control group (n = 6) and four cervical spondylotic myelopathy (CSM) groups (n = 6 per time point). Chronic cervical spinal cord compression was induced by implanting a hydrophilic polyurethane polymer sheet into the C5–C6 epidural space. CSM rats were evaluated at 1 week, 2 weeks, 1 month, and 2 months after compression. Magnetic resonance imaging (MRI) was performed to confirm spinal cord compression and exclude intramedullary hemorrhage or edema. Neurological function was evaluated using the Basso–Beattie–Bresnahan (BBB) locomotor scale and somatosensory evoked potential (SEP) recordings. Gray- and white-matter pathology was assessed using hematoxylin and eosin (HE) and Luxol fast blue (LFB) staining, respectively. Transmission electron microscopy (TEM) was used to characterize ultrastructural alterations in neurons, axons, myelin sheaths, mitochondria, and microvessels.

Results:

(1) MRI confirmed sustained dorsolateral cervical spinal cord compression without intramedullary edema or hemorrhage. BBB scores decreased markedly during the first week and stabilized at approximately 16–17 by 1 month, whereas SEP latency remained prolonged and amplitude remained reduced. (2) Histological analysis showed progressive anterior horn motor neuron loss and dorsal column myelin damage. At 1 month, motor neuron counts had decreased to 13.83 ± 0.70, the myelinated area to 86.21 ± 2.36%, and the vacuolated area had increased to 13.79 ± 2.36% ($P \leq 0.001$). (3) TEM revealed progressive mitochondrial degeneration, axon–myelin disruption, and microvascular narrowing. At 1 month, mitochondrial cristae had decreased to 4.30 ± 0.16 per profile, and the microvascular lumen-to-cross-sectional area ratio had declined to 31.00 ± 1.42%. These abnormalities persisted or progressed at 2 months, demonstrating that the pathological phenotype was established by 1 month.

Conclusion:

Cervical cord injury progressed in a time-dependent manner, and 1 month of compression may represent a critical pathological window for the CSM model.

Introduction

Cervical spondylotic myelopathy (CSM) is a chronic compressive disorder of the cervical spinal cord resulting from degenerative cervical spine changes, including intervertebral disc herniation, osteophyte formation, and hypertrophy or ossification of the posterior longitudinal ligament[1–3]. These changes can cause static or dynamic mechanical compression, impair local spinal cord perfusion, and lead to progressive neurological dysfunction[4–6].Although surgical decompression is the standard treatment for symptomatic CSM, clinical decision-making remains challenging. The extent of spinal cord compression on magnetic resonance imaging does not consistently correlate with neurological impairment, the optimal timing of surgery remains uncertain, and postoperative recovery varies considerably among patients.[2, 4, 7]. These discrepancies suggest that CSM progression depends not only on static compression but also on time-dependent pathological changes within the spinal cord. However, their temporal sequence remains poorly defined, limiting the identification of an optimal therapeutic window [7–9].

Experimental models are essential for investigating the temporal pathophysiology of CSM because serial pathological assessment is not feasible in patients[7, 10]. Several rat models of chronic cervical spinal cord compression have been developed, including expandable polymer, synthetic polyether, and polyvinyl alcohol–polyacrylamide hydrogel models[8, 11–13]. However, compression duration and pathological outcomes vary substantially because of differences in model design, material properties, compression severity, anatomical level, and outcome measures [7, 12, 13]. Consequently, no consensus has been reached on the time point at which a CSM rat model can be considered successfully established, as neurological, electrophysiological, and pathological abnormalities emerge at different stages across models [6, 7, 12, 13]. Our group established a rat model of gradual cervical spinal cord compression using a hydrophilic polyurethane polymer implanted into the C5–C6 epidural space, where it expands to a stable volume and maintains sustained compression[14, 15]. Previous studies using this model have demonstrated spinal cord deformation, electrophysiological abnormalities, neuronal loss, vacuolation, axonal degeneration, demyelination, microvascular remodeling, neurovascular unit disruption, and partial spontaneous functional recovery[12, 14–17]. Nevertheless, the temporal relationships among neurological dysfunction, histopathological injury, and ultrastructural alterations remain unclear. Therefore, this study aimed to characterize these changes over time and identify a reproducible pathological window for successful model establishment.

Materials and methods

Animals and experimental CSM model

Thirty 2-month-old female Sprague–Dawley rats weighing 200–302 g were used in this study. Animals were randomly assigned to either the CSM group (n = 24) or the sham-operated control group (n = 6). Rats in the CSM group were euthanized at 1 week, 2 weeks, 1 month,and 2 months after compression, with six rats examined at each time point. All procedures were conducted in accordance with the Guide

for the Care and Use of Laboratory Animals and were approved by the institutional animal ethics committee.

The CSM model was established according to the method described by Li et al[15].. A hydrophilic polyurethane polymer sheet (Shenzhen Fulin, China) was used as the compression-inducing material. After water absorption, the material gradually expanded within 24 h, thereby producing slow and sustained compression that mimics the progressive nature of human CSM.Rats were anesthetized by intraperitoneal injection of ketamine (40 mg/kg) and xylazine (5 mg/kg) (Sigma-Aldrich, USA). The C5 vertebral level was identified by radiography. Through a posterior midline cervical incision, the left C5 lamina was exposed. After C5 laminectomy, the C5–C6 epidural space was exposed and the dura was carefully visualized. Under an operating microscope, a sterilized polymer sheet was inserted into the left C5–C6 epidural space while avoiding injury to the dura or spinal cord. Sham-operated rats underwent the same surgical exposure without polymer implantation. The wound was closed in layers, and animals were allowed to recover on a thermostatically controlled heating pad before being housed separately. General condition was monitored daily, and neurological assessments were performed at predefined time points. All animals survived until their scheduled endpoints.

Neurological assessment

Hindlimb locomotor function was assessed using the Basso–Beattie–Bresnahan (BBB) locomotor scale preoperatively and at 1 day, 3 days, 1 week, 2 weeks, 3 weeks, 1 month,and 2 months after surgery. Two spine surgeons blinded to group allocation performed scoring independently, and the average score was used for analysis.

Somatosensory evoked potentials (SEPs) were recorded to assess sensory conduction. The tibial nerve was stimulated at 5.1 Hz with a pulse duration of 0.2 ms. Cortical responses were recorded from the Cz–Fz derivation according to the international 10–20 system using a YRKJ-G2008 electrophysiological system (Zhuhai Yiren Technology, Zhuhai, China). Signals were amplified 100,000-fold, band-pass filtered at 20–2000 Hz, and averaged over 200 responses. SEP latency was defined as the interval from stimulation onset to the first negative peak (N1). SEP amplitude was defined as the P1–N1 peak-to-peak voltage difference.

Tissue preparation and histology

At each endpoint, rats were euthanized with an overdose of intraperitoneal sodium pentobarbital. The cervical spinal cord was removed en bloc and fixed in phosphate-buffered 4% paraformaldehyde for 24 h. A 5-mm segment centered on the C5 compression site was harvested, processed, embedded in paraffin, and sectioned longitudinally at 5 μm.

Sections were stained with hematoxylin and eosin (HE) or Luxol fast blue (LFB). Images were acquired using an Olympus FV-1000 microscope (Olympus, Japan) and analyzed with ImageJ 1.47v software

(National Institutes of Health, USA). Large motor neurons in the ventral gray matter with a soma diameter > 20 μm were counted at 10× magnification. Myelin and vacuolar contents in the posterior funiculus were estimated by quantifying LFB-positive staining in ×20 microscopic images using ImageJ software.

Transmission electron microscopy

Selected spinal cord samples were processed for transmission electron microscopy (TEM). Ultrathin sections were double-stained with uranyl acetate and lead citrate, examined using a JEM-1400 transmission electron microscope, and imaged with a GATAN 832 system (Gatan, USA).

Ultrastructural parameters were quantified using ImageJ 1.47v (National Institutes of Health, USA) and MyelTracer. ImageJ was used to measure the number of mitochondrial cristae in neuronal mitochondria at 60,000× magnification and the microvascular lumen-to-cross-sectional area ratio at 8,000× magnification. Normal and degenerative mitochondria in neurons and axons were counted and normalized to tissue area to calculate mitochondrial densities. Myelin sheath thickness and the g-ratio, defined as the ratio of the inner axonal diameter to the outer fiber diameter, were measured at 8,000× magnification using MyelTracer.

Statistical analysis

Statistical analyses were performed using SPSS version 25.0 (IBM Corp., Armonk, NY, USA). Data are presented as the mean ± SEM. Multiple-group comparisons were conducted using one-way ANOVA with Tukey's post hoc test for equal variances or Welch's ANOVA with Tamhane's T2 test for unequal variances. Left–right differences in large motor neuron counts were assessed using repeated-measures ANOVA. All tests were two-sided, with $P < 0.05$ considered statistically significant.

Results

Chronic compression induces neurological dysfunction

MRI confirmed that the expanded polymer produced sustained dorsolateral compression of the cervical spinal cord at C5–C6 in CSM rats, resulting in visible cord deformation on both T1- and T2-weighted images without evidence of intramedullary edema, hemorrhage, or abnormal parenchymal signal at the compression site (Fig. 1C,D).

Chronic compression induces time-dependent neurological and electrophysiological deficits

Basso–Beattie–Bresnahan (BBB) locomotor scores. (B) Somatosensory evoked potential (SEP) latency. (C) SEP amplitude. "*" Compared with preoperative, "#" compared with postoperative($P < 0.05$)

BBB scores declined sharply after compression and then partially recovered (Fig. 2A). After compression, rats showed impaired weight support, unstable plantar stepping, and poor limb coordination. BBB scores decreased from 21 preoperatively to approximately 11–12 between day 1 and week 1, then increased to approximately 16–17 at 1 month and changed little thereafter (Fig. 2A). SEP latency was initially prolonged but shortened at 1 month, with a significant reduction from the early postoperative value ($P < 0.05$; Fig. 2B). SEP amplitudes decreased bilaterally, particularly on the right, and remained significantly below baseline at 1 month despite partial recovery from the week-1 minimum ($P < 0.05$; Fig. 2C). Thus, at 1 month, locomotor function had largely stabilized, whereas SEP abnormalities persisted.

Time-dependent histopathological features after chronic compression

HE staining revealed progressive ventral horn damage after chronic compression (Fig. 3D, E). Controls showed preserved tissue architecture and numerous large motor neurons with intact cell bodies and clearly visible nuclei. After compression, motor neurons were reduced and irregularly distributed, with cell shrinkage, cytoplasmic vacuolation, and tissue rarefaction. These changes were prominent at 1 month and persisted at 2 months. Quantitative analysis showed a time-dependent decrease in motor neuron counts, from approximately 34 in controls to 13.83 ± 0.70 at 1 month, and 12.00 ± 0.68 at 2 months (Welch's ANOVA, $P < 0.001$). Counts also differed significantly between the anterior horns ($P < 0.001$), with greater neuronal loss on the compressed left side. At 2 months, significantly fewer motor neurons remained in the left anterior horn than in the right ($P < 0.01$).

LFB staining showed compact and uniformly stained myelin in the dorsal column of control rats, whereas CSM rats exhibited fiber disruption, disorganization, widened inter-fiber spaces, and vacuolation (Fig. 3C). The percentage of myelinated area in the dorsal column decreased over time after compression ($P <= 0.001$, one-way ANOVA). At 1 month, the myelinated area had decreased to 86.21 ± 2.36%, accompanied by focal pallor, fiber separation, and disorganization, indicating that myelin disruption was already evident within the 1-month pathological window. This reduction progressed further at 2 months, when the vacuolated area reached its lowest value of 13.83 ± 0.94%. In contrast, the vacuolated area increased over time ($P = 0.001$, one-way ANOVA), rising to 13.79 ± 2.36% at 1 month and further increasing to 13.83 ± 0.94% at 2 months. These changes indicate that, after sustained cervical spinal cord compression, the myelinated area in the dorsal column progressively decreased, whereas the vacuolated area continuously expanded.

Time-dependent ultrastructural features after compression

TEM revealed progressive ultrastructural degeneration after chronic compression, including mitochondrial abnormalities, axonal and myelin disruption, and microvascular narrowing (Fig. 4). In control rats, neuronal mitochondria had intact membranes and well-defined cristae, while microvessels showed regular contours, patent lumina, and thin, continuous endothelial walls. After compression,

morphologically normal mitochondria gradually decreased, whereas swelling, vacuolation, and cristae disruption became increasingly evident. Microvessels also became irregular, with endothelial swelling, wall thickening, and progressive luminal narrowing; some vessels showed marked deformation or partial collapse. By 1 month, mitochondrial degeneration and microvascular stenosis were prominent, with fewer normal mitochondria and smaller vascular lumina. These abnormalities persisted at 2 months (Fig. 4A).

Quantitative TEM analysis confirmed time-dependent mitochondrial alterations in neuronal somata after chronic compression (Fig. 4E,F). The density of normal mitochondria in motor neurons decreased significantly over time ($P < 0.001$, Welch's ANOVA; Fig. 4E), falling to $0.08 \pm 0.02/\mu m^2$ at 1 month and $0.10 \pm 0.03/\mu m^2$ at 2 months. Conversely, the density of degenerative mitochondria increased progressively ($P < 0.001$, Welch's ANOVA; Fig. 4F), reaching $0.56 \pm 0.01/\mu m^2$ at 1 month and $0.61 \pm 0.04/\mu m^2$ at 2 months. These findings show that neuronal mitochondrial degeneration was already evident within the 1-month pathological window and progressed thereafter.

Axonal and myelin structures showed parallel time-dependent deterioration after chronic compression. Control axons displayed regular neurofilaments, microtubules, and compact myelin lamellae. At 1 week, neurofilament disorganization and focal myelin loosening were observed, followed by axoplasmic rarefaction, neurofilament loss, myelin separation, and vacuolation at 2 weeks. By 1 month, axonal contours became poorly defined, with marked myelin loosening, splitting, and focal disruption. These abnormalities persisted at 2 months (Fig. 4B).

Axonal mitochondria in the spinal white matter showed a similar pattern of deterioration (Fig. 4G,H). Normal axonal mitochondrial density decreased significantly after compression ($P < 0.001$, Welch's ANOVA; Fig. 4G), whereas degenerative axonal mitochondrial density increased over time ($P < 0.001$, Welch's ANOVA; Fig. 4H). By 1 month, normal axonal mitochondrial density had decreased to $0.15 \pm 0.01/\mu m^2$, while degenerative mitochondrial density had increased to $0.54 \pm 0.05/\mu m^2$, indicating established axonal mitochondrial abnormalities at this time point.

Axon–myelin measurements also changed significantly during chronic compression (Fig. 4I,J). The axonal g-ratio showed significant temporal variation ($P < 0.001$, one-way ANOVA; Fig. 4I), measuring 0.67 ± 0.01 at 1 month and increasing further to 0.72 ± 0.01 at 2 months. Myelin sheath thickness also differed among groups ($P < 0.01$, one-way ANOVA; Fig. 4J), showing a transient increase at 1 month (0.82 ± 0.06 μm), followed by a marked decrease at 2 months (0.67 ± 0.04 μm). These results indicate dynamic axon–myelin structural changes during disease progression.

Mitochondrial cristae and microvascular structure showed additional time-dependent deterioration (Fig. 4K,L). The number of cristae per intraneuronal mitochondrial profile decreased significantly after compression ($P < 0.001$, one-way ANOVA; Fig. 4K), falling from 7.20 ± 0.51 in controls to 4.30 ± 0.16 at 1 month and 4.02 ± 0.21 at 2 months. The ratio of luminal area to total microvascular area also decreased significantly ($P = 0.001$, one-way ANOVA; Fig. 4L), reaching $31.00 \pm 1.42\%$ at 1 month and $22.84 \pm 8.36\%$

at 2 months. Together, these quantitative findings demonstrate that mitochondrial, axonal–myelin, and microvascular abnormalities were established by 1 month and progressed at later stages.

Discussion

CSM is a chronic compressive disorder of the cervical spinal cord, but its progression cannot be explained by mechanical compression alone. The mismatch among clinical symptoms, imaging findings, and postoperative recovery suggests that ischemia–hypoxia, blood–spinal cord barrier disruption, neuronal degeneration, axonal demyelination, mitochondrial dysfunction, and neurovascular unit impairment may jointly contribute to disease progression [14, 15, 18, 19]. In this study, we systematically examined the time-dependent neurological, histopathological, and ultrastructural alterations induced by chronic cervical spinal cord compression in a rat model of experimental CSM. Locomotor dysfunction appeared early and partially recovered, whereas SEP abnormalities persisted. Anterior horn neuronal loss, dorsal column myelin disruption, mitochondrial degeneration, axonal and myelin alterations, and microvascular narrowing were evident by 1 month and progressed thereafter. Our study demonstrates that 1 month after compression as a reliable experimental window for established chronic compression-induced cervical myelopathy in this rat model.

Human autopsy findings provide an important benchmark for evaluating the pathological relevance of experimental CSM models. Autopsy specimens from patients with CSM show anterior horn neuronal loss, white matter demyelination, axonal loss, gliosis, cavitation, and necrosis, indicating involvement of both gray and white matter[10, 20–22]. Fehlings and colleagues developed a rat model of CSM by implanting a synthetic aromatic polyether beneath the C6 lamina to induce chronic progressive cervical spinal cord compression. However, they did not identify a specific time point at which the pathological phenotype became established[11]. To our knowledge, the present study is to show that 1 month of chronic compression is sufficient to establish a reproducible pathological phenotype of CSM in rats. This time point should therefore be regarded as a reproducible stage specific to this model, rather than as a direct temporal equivalent of human disease.

Behavioral and electrophysiological outcomes followed divergent trajectories after chronic compression. BBB scores decreased from 21 to approximately 11–12 between postoperative day 1 and week 1, indicating marked early locomotor impairment, and subsequently recovered to approximately 16 at 1 month and 17 at 2 months. However, the score remained below baseline at 1 month, while SEP latency remained prolonged and amplitude remained reduced, indicating persistent somatosensory conduction impairment. This dissociation likely reflects the different functional domains assessed by these measures. BBB scoring evaluates gross hindlimb locomotion, which may improve through recruitment of spared pathways, reorganization of spinal networks, and compensatory changes at adjacent spinal levels[14, 23]. By contrast, SEP recordings are more sensitive to dysfunction of ascending sensory pathways. Persistent axonal and myelin injury may slow conduction and reduce neural synchrony, resulting in prolonged latency and reduced amplitude despite partial locomotor recovery[15, 17]. These electrophysiological deficits are consistent with the progressive axonal, myelin, mitochondrial, and

microvascular abnormalities observed in the compressed spinal cord in this study.Thus, the improvement in BBB scores likely reflects partial functional compensation rather than structural or electrophysiological recovery. These findings support the combined use of behavioral and electrophysiological assessments in experimental CSM[23, 24]. The coexistence of partial locomotor recovery and persistent conduction deficits at 1 month indicates established neurological dysfunction rather than functional resolution.

Histological and ultrastructural analyses further defined the transition from early functional impairment to established structural degeneration. HE staining showed progressive loss of large anterior horn motor neurons, with greater loss on the compressed side, consistent with the dorsolateral compression produced by the implanted polymer. LFB staining revealed parallel posterior column deterioration, characterized by reduced myelin staining, fiber disorganization, widened spaces between fibers, and progressive vacuolation. By 1 month, both gray and white matter abnormalities were clearly established. TEM confirmed this pathological trajectory. Neuronal and axonal mitochondria showed progressive degeneration with reduced cristae integrity, while axons and myelin exhibited loosening, splitting, focal disruption, and vacuolar change. These ultrastructural findings are consistent with previous TEM studies of experimental CSM, which reported neurovascular unit disruption, mitochondrial degeneration, axonal and myelin damage, and microvascular alterations after chronic cervical cord compression[14, 15]. At 1 month, mitochondrial degeneration, myelin decompaction, and axon–myelin disruption coexisted with increased myelin sheath thickness and a relatively low g-ratio.This pattern likely reflects reactive swelling or unstable remodeling of axons and myelin rather than effective remyelination. Later stages showed more severe myelin loss and axonal degeneration, indicating progressive deterioration of both myelin and axonal structures after the 1 month stage.

Microvascular pathology was another key feature of the temporal changes induced by chronic compression. TEM showed progressive vascular distortion, characterized by luminal narrowing and vascular wall abnormalities. These changes were evident at 1 month and became more severe thereafter, suggesting gradual loss of microvascular patency in the compressed spinal cord. At the 1 month stage, microvascular narrowing occurred together with mitochondrial degeneration, axonal disruption, myelin damage, and posterior column white matter deterioration. This pattern suggests that impaired local perfusion, hypoxia, and ischemic stress may contribute to neuronal energy failure, axonal vulnerability, and myelin degeneration.Previous studies have reported blood–spinal cord barrier disruption and neurovascular unit abnormalities in CSM, involving endothelial cells, pericytes, astrocytic endfeet, and oligodendrocytes [14, 15, 18]. Thus, the microvascular abnormalities observed at 1 month may represent an early stage of vascular decompensation that links chronic mechanical compression to coordinated neurovascular and parenchymal pathology.

Taken together, this chronic cervical spinal cord compression model demonstrated progressive experimental cervical myelopathy in rats. Early compression caused marked locomotor impairment and persistent electrophysiological dysfunction.At 1 month, BBB scores showed only partial recovery, whereas SEP abnormalities persisted. Histological and ultrastructural abnormalities were also

established at this stage, including anterior horn motor neuron loss, dorsal column myelin disruption, mitochondrial degeneration, axonal and myelin damage, and microvascular pathology. These changes progressed further at later time points. Thus, 1 month after compression represents a reliable experimental window for established cervical myelopathy induced by chronic compression, rather than the endpoint of disease progression.

Although the model reproduced key pathological features of chronic cervical spinal cord compression, differences between rats and humans in lifespan, spinal anatomy, biomechanics, and disease progression limit direct extrapolation to human CSM. One month in an adult rat has been estimated to correspond to approximately 2.5 human years; however, this relationship varies according to developmental stage and the biological process under investigation and should not be interpreted as a direct chronological equivalence[25] .

Declarations

Data availability statement

The original data and contributions generated in this study are provided within the article and its supplementary materials. Any additional questions may be addressed to the corresponding author.

Ethics statement

The experimental protocol involving animals was assessed and approved by the Animal Experiment Ethics Committee at Guangdong Medical University's Affiliated Hospital.

Author contributions

S- HO and XS contributed to the study conception and design and drafted the manuscript. S-HO, G-SL, S-JN, R-HLand H-XS conducted the experiments. S-HO and L-C collected the data, and S-HO performed the data analysis. XS critically reviewed and revised the manuscript. All authors read and approved the final manuscript.

Funding

This study was funded by the Natural Science Foundation of Guangdong Province, China (2018A0303130105 and 2016A030313679), and the Zhanjiang Municipal Science and Technology Bureau (2025A502017). The funding bodies had no role in the study design, experimental implementation, data acquisition or analysis, the decision to submit the work for publication, or manuscript preparation.

Conflict of interest

The authors confirm that no commercial or financial affiliations existed during the conduct of this research that could be regarded as a potential conflict of interest.

Publisher's note

All opinions and claims made in this article are the responsibility of the authors alone and should not be taken as representing the views of their institutions, the publisher, the editors, or the reviewers. Any product discussed or evaluated herein, as well as any manufacturer's claim, is neither guaranteed nor endorsed by the publisher.

References

1. McCormick JR, Sama AJ, Schiller NC, Butler AJ, Donnally CJ, 3rd. Cervical Spondylotic Myelopathy: A Guide to Diagnosis and Management. J Am Board Fam Med. 2020;33(2):303–13. doi: 10.3122/jabfm.2020.02.190195. PubMed PMID: 32179614.
2. Badhiwala JH, Ahuja CS, Akbar MA, Witiw CD, Nassiri F, Furlan JC, et al. Degenerative cervical myelopathy - update and future directions. Nat Rev Neurol. 2020;16(2):108–24. Epub 20200123. doi: 10.1038/s41582-019-0303-0. PubMed PMID: 31974455.
3. Nouri A, Tetreault L, Singh A, Karadimas SK, Fehlings MG. Degenerative Cervical Myelopathy: Epidemiology, Genetics, and Pathogenesis. Spine (Phila Pa 1976). 2015;40(12):E675–93. doi: 10.1097/brs.0000000000000913. PubMed PMID: 25839387.
4. Karadimas SK, Gatzounis G, Fehlings MG. Pathobiology of cervical spondylotic myelopathy. Eur Spine J. 2015;24 Suppl 2:132–8. Epub 20140314. doi: 10.1007/s00586-014-3264-4. PubMed PMID: 24626958.
5. Tu J, Vargas Castillo J, Das A, Diwan AD. Degenerative Cervical Myelopathy: Insights into Its Pathobiology and Molecular Mechanisms. J Clin Med. 2021;10(6). Epub 20210315. doi: 10.3390/jcm10061214. PubMed PMID: 33804008; PubMed Central PMCID: PMC8001572.
6. Ren ZX, Xu JH, Cheng X, Xu GX, Long HQ. Pathophysiological mechanisms of chronic compressive spinal cord injury due to vascular events. Neural Regen Res. 2023;18(4):790–6. doi: 10.4103/1673-5374.353485. PubMed PMID: 36204839; PubMed Central PMCID: PMC9700100.
7. Akter F, Yu X, Qin X, Yao S, Nikrouz P, Syed YA, et al. The Pathophysiology of Degenerative Cervical Myelopathy and the Physiology of Recovery Following Decompression. Front Neurosci. 2020;14:138. Epub 20200430. doi: 10.3389/fnins.2020.00138. PubMed PMID: 32425740; PubMed Central PMCID: PMC7203415.
8. Kim P, Haisa T, Kawamoto T, Kirino T, Wakai S. Delayed myelopathy induced by chronic compression in the rat spinal cord. Ann Neurol. 2004;55(4):503–11. doi: 10.1002/ana.20018. PubMed PMID: 15048889.
9. Kasahara K, Nakagawa T, Kubota T. Neuronal loss and expression of neurotrophic factors in a model of rat chronic compressive spinal cord injury. Spine (Phila Pa 1976). 2006;31(18):2059–66. doi: 10.1097/01.brs.0000231893.21964.f2. PubMed PMID: 16915089.
10. Dohle E, Beardall S, Chang A, Mena KPC, Jovanović L, Nath U, et al. Human spinal cord tissue is an underutilised resource in degenerative cervical myelopathy: findings from a systematic review of

human autopsies. Acta Neurochir (Wien). 2023;165(5):1121–31. Epub 20230223. doi: 10.1007/s00701-023-05526-5. PubMed PMID: 36820887; PubMed Central PMCID: PMC10140111.

11. Karadimas SK, Moon ES, Yu WR, Satkunendrarajah K, Kallitsis JK, Gatzounis G, et al. A novel experimental model of cervical spondylotic myelopathy (CSM) to facilitate translational research. Neurobiol Dis. 2013;54:43–58. Epub 20130304. doi: 10.1016/j.nbd.2013.02.013. PubMed PMID: 23466695.
12. Long HQ, Li GS, Lin EJ, Xie WH, Chen WL, Luk KD, et al. Is the speed of chronic compression an important factor for chronic spinal cord injury rat model? Neurosci Lett. 2013;545:75–80. Epub 20130428. doi: 10.1016/j.neulet.2013.04.024. PubMed PMID: 23632138.
13. Ijima Y, Furuya T, Koda M, Matsuura Y, Saito J, Kitamura M, et al. Experimental rat model for cervical compressive myelopathy. Neuroreport. 2017;28(18):1239–45. doi: 10.1097/wnr.0000000000000907. PubMed PMID: 28957944; PubMed Central PMCID: PMC5704668.
14. Li GS, Chen GH, Wang KH, Wang XX, Hu XS, Wei B, et al. Neurovascular Unit Compensation from Adjacent Level May Contribute to Spontaneous Functional Recovery in Experimental Cervical Spondylotic Myelopathy. Int J Mol Sci. 2023;24(4). Epub 20230208. doi: 10.3390/ijms24043408. PubMed PMID: 36834841; PubMed Central PMCID: PMC9962900.
15. Li GS, Wang XX, Tan RB, Wang KH, Hu XS, Hu Y. Ultrastructural destruction of neurovascular unit in experimental cervical spondylotic myelopathy. Front Neurosci. 2022;16:1031180. Epub 20221116. doi: 10.3389/fnins.2022.1031180. PubMed PMID: 36466180; PubMed Central PMCID: PMC9709118.
16. Cheng X, Long H, Chen W, Xu J, Huang Y, Li F. Three-dimensional alteration of cervical anterior spinal artery and anterior radicular artery in rat model of chronic spinal cord compression by micro-CT. Neurosci Lett. 2015;606:106–12. Epub 20150905. doi: 10.1016/j.neulet.2015.08.050. PubMed PMID: 26327142.
17. Li GS, Li HQ, Hu Y, Wang CY, Li SY, Li FB. Pathological mechanism of neurofilament hyperphosphorylation-mediated somatosensory evoked potential abnormalities in chronic compressive cervical spinal cord injury. J Sun Yat-sen Univ Med Sci. 2012;33:28. Chinese..
18. Kim HW, Yong H, Shea GKH. Blood-spinal cord barrier disruption in degenerative cervical myelopathy. Fluids Barriers CNS. 2023;20(1):68. Epub 20230925. doi: 10.1186/s12987-023-00463-y. PubMed PMID: 37743487; PubMed Central PMCID: PMC10519090.
19. Vallotton K, David G, Hupp M, Pfender N, Cohen-Adad J, Fehlings MG, et al. Tracking White and Gray Matter Degeneration along the Spinal Cord Axis in Degenerative Cervical Myelopathy. J Neurotrauma. 2021;38(21):2978–87. Epub 20210803. doi: 10.1089/neu.2021.0148. PubMed PMID: 34238034.
20. Ito T, Oyanagi K, Takahashi H, Takahashi HE, Ikuta F. Cervical spondylotic myelopathy. Clinicopathologic study on the progression pattern and thin myelinated fibers of the lesions of seven

patients examined during complete autopsy. Spine (Phila Pa 1976). 1996;21(7):827–33. doi: 10.1097/00007632-199604010-00010. PubMed PMID: 8779013.

21. Iwabuchi M, Kikuchi S, Sato K. Pathoanatomic investigation of cervical spondylotic myelopathy. Fukushima J Med Sci. 2004;50(2):47–54. doi: 10.5387/fms.50.47. PubMed PMID: 15779570.
22. Someya Y, Koda M, Hashimoto M, Okawa A, Masaki Y, Yamazaki M. Postmortem findings in a woman with history of laminoplasty for severe cervical spondylotic myelopathy. J Spinal Cord Med. 2011;34(5):523–6. doi: 10.1179/107902611x13069205199503. PubMed PMID: 22118261; PubMed Central PMCID: PMC3184491.
23. Lee J, Satkunendrarajah K, Fehlings MG. Development and characterization of a novel rat model of cervical spondylotic myelopathy: the impact of chronic cord compression on clinical, neuroanatomical, and neurophysiological outcomes. J Neurotrauma. 2012;29(5):1012–27. Epub 20110829. doi: 10.1089/neu.2010.1709. PubMed PMID: 21561323.
24. Tracy JA, Bartleson JD. Cervical spondylotic myelopathy. Neurologist. 2010;16(3):176–87. doi: 10.1097/NRL.0b013e3181da3a29. PubMed PMID: 20445427.
25. Andreollo NA, Santos EF, Araújo MR, Lopes LR. Rat's age versus human's age: what is the relationship? Arq Bras Cir Dig. 2012;25(1):49–51. doi: 10.1590/s0102-67202012000100011. PubMed PMID: 22569979.

Figures

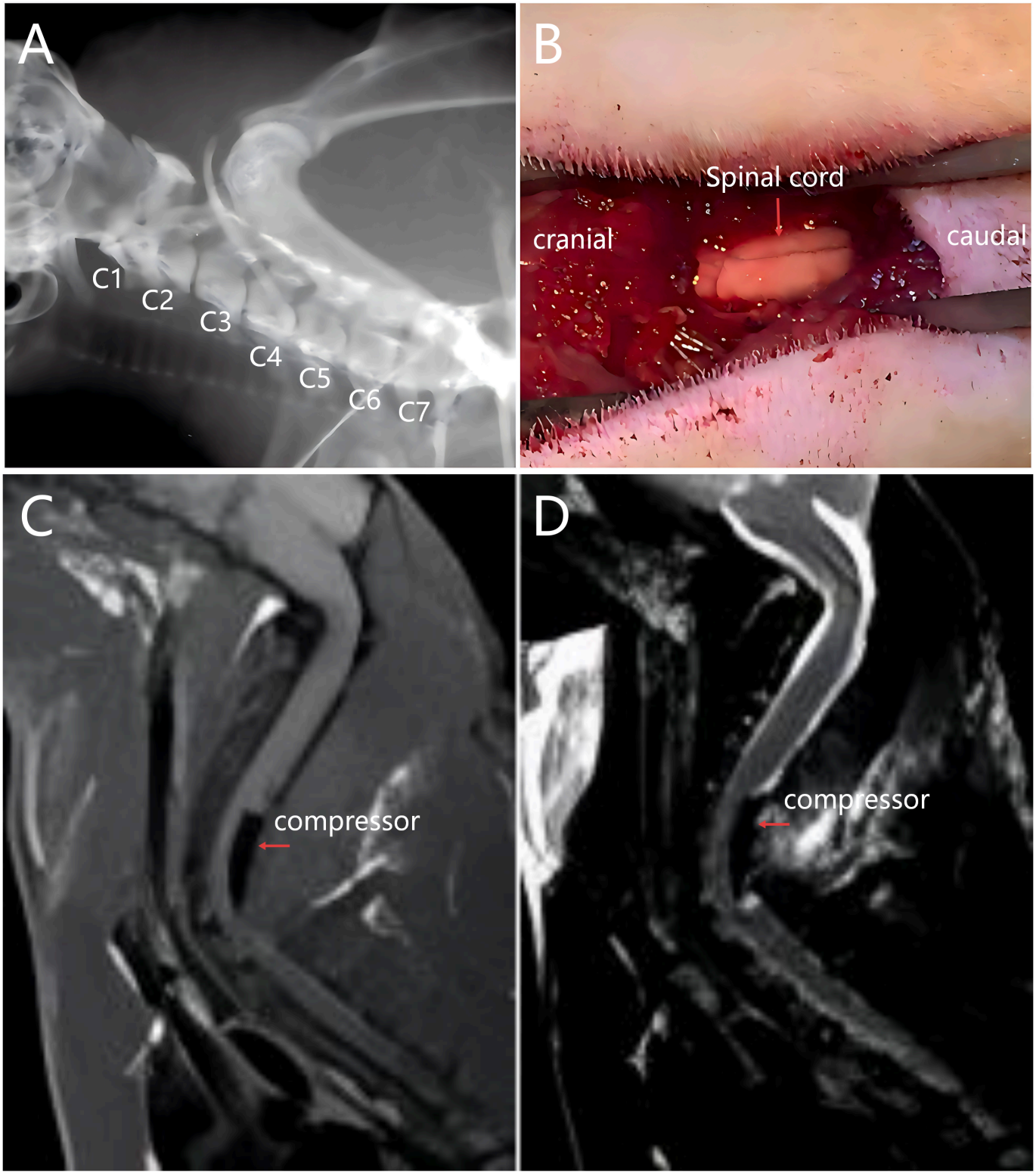

Figure 1

Generation of an experimental rat model of CSM.

(A) X-ray localization of the C5 vertebral level.(B) C5–C6 epidural space exposed after C5 laminectomy. (C) Sagittal T1-weighted MRI of a rat with CSM.(D) Sagittal T2-weighted MRI of a rat with CSM.

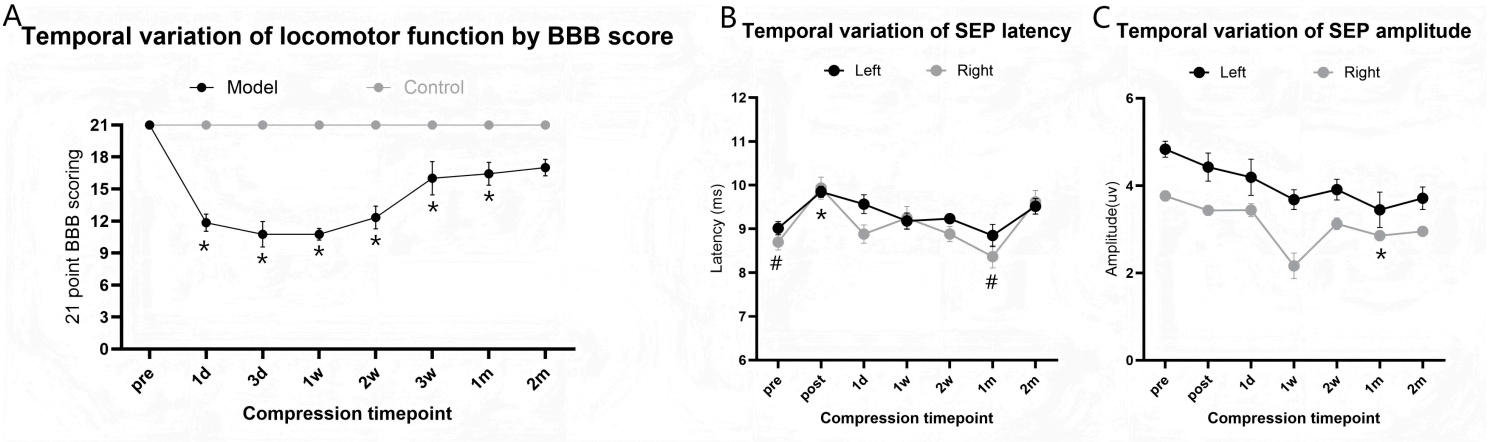

Figure 2

Time-dependent neurological changes in CSM rats.

(A) Basso–Beattie–Bresnahan (BBB) locomotor scores. (B) Somatosensory evoked potential (SEP) latency. (C) SEP amplitude. “*” Compared with preoperative, “#” compared with postoperative P<0.05)

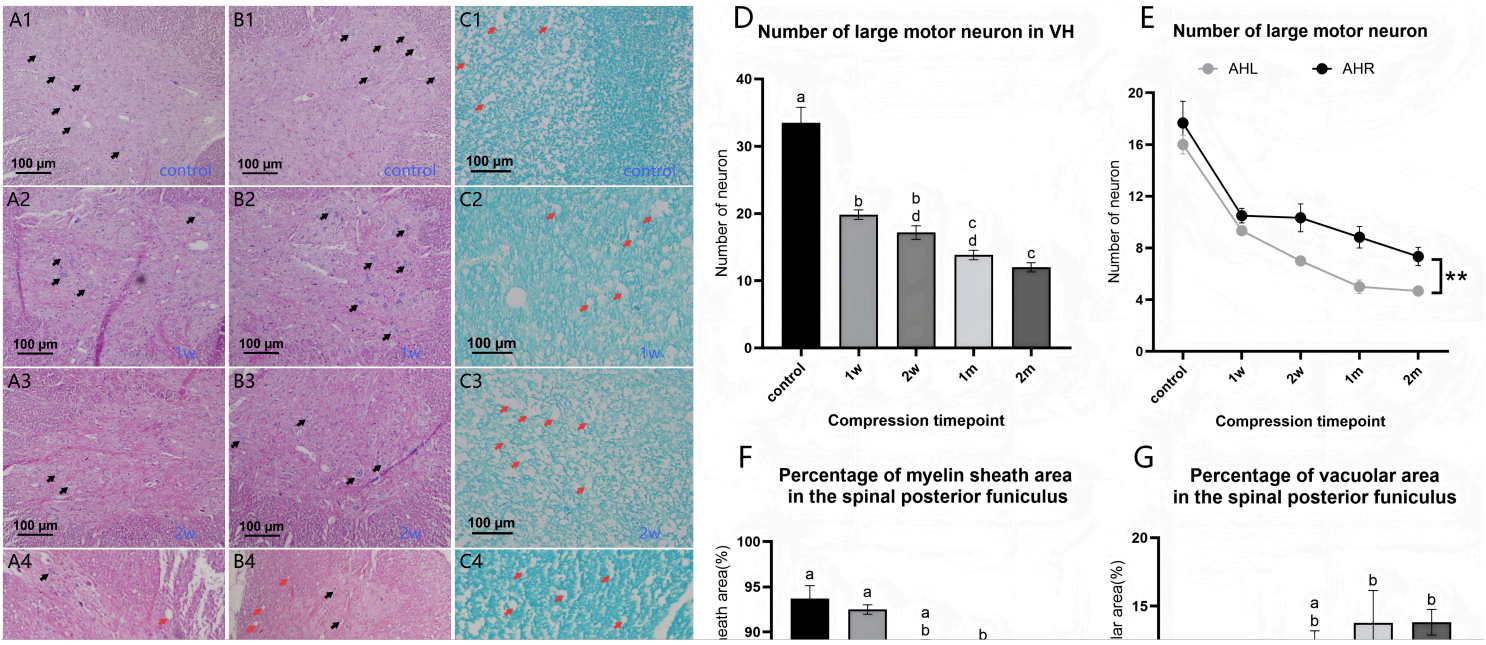

Figure 3

Time-dependent histological changes in the cervical spinal cord.

A1–A5, HE staining of the left anterior horn in control rats and rats compressed for 1 week, 2 weeks, 1 month and 2 months. B1–B5, HE staining of the right anterior horn at the same time points. C1–C5, LFB staining of the dorsal column showing nerve fibers and vacuolation. D, total anterior horn motor neuron counts. E, left and right anterior horn motor neuron counts. F,Percentage of myelinated area in the dorsal column. G,Percentage of vacuolated area in the dorsal column.. Black arrows indicate large motor neurons; red arrows indicate vacuoles. Different letters indicate P < 0.05; **P < 0.01.

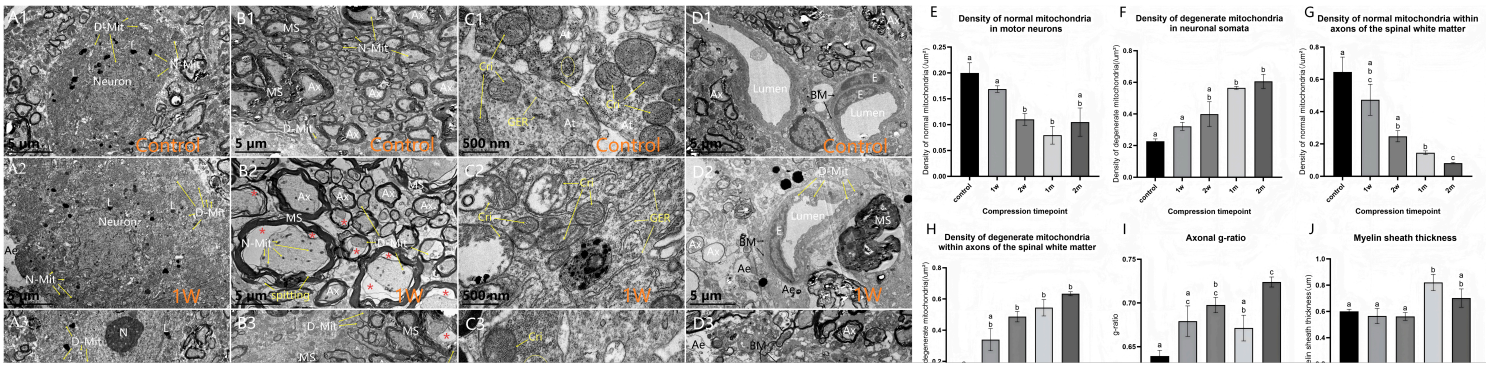

Figure 4

Time-dependent ultrastructural changes in the cervical spinal cord after chronic compression.(A1–A5) Neuronal mitochondria. (B1–B5) Axonal mitochondria and myelin ultrastructure. (C1–C5) Mitochondrial cristae. (D1–D5) Microvascular ultrastructure. Images correspond to control rats and rats compressed for 1 week, 2 weeks, 1 month, and 2 months. (E,F) Quantification of normal and degenerative neuronal mitochondrial densities. (G,H) Quantification of normal and degenerative axonal mitochondrial densities. (I) Axonal g-ratio. (J) Myelin sheath thickness. (K) Number of mitochondrial cristae. (L) Ratio of luminal area to total microvascular area. N, nucleus; N-Mit, normal mitochondrion; D-Mit, degenerative mitochondrion; Ax, axon; MS, myelin sheath; At, axon terminal; SC, synaptic cleft; SV, synaptic vesicle; D, dendrite; M, mitochondrion; Cri, mitochondrial crista; L, lysosome; GER, granular endoplasmic reticulum; E, endothelial cell; P, pericyte; BM, basement membrane; Ae, astrocytic endfoot. Yellow ovals indicate synaptic vesicles; asterisks indicate axonal vacuolation. Data are presented as the mean ± SEM. Different letters indicate significant differences among groups (P < 0.05).